Chapter 11

Dynamics-Function Analysis in Catalytic RNA Using NMR Spin Relaxation and Conformationally Restricted Nucleotides

Charles G. Hoogstraten, Montserrat Terrazas, Anna Aviñó, Neil A. White, and Minako Sumita

Abstract

A full understanding of biomolecular function requires an analysis of both the dynamic properties of the system of interest and the identification of those dynamics that are required for function. We describe NMR methods based on metabolically directed specific isotope labeling for the identification of molecular disorder and/or conformational transitions on the RNA backbone ribose groups. These analyses are complemented by the use of synthetic covalently modified nucleotides constrained to a single sugar pucker, which allow functional assessment of dynamics by selectively removing a minor conformer identified by NMR from the structural ensemble.

Key words Conformational restriction, NMR dynamics, Noncoding RNA, Dynamics-function, Sugar pucker

1 Introduction

A complete understanding of the function of biological macromolecules and their assemblies requires detailed study of both three-dimensional structures and of the time-dependent properties of those structures, i.e., molecular dynamics, as well as the correlation of both types of properties with biological function. The structure-function paradigm, in which three-dimensional structural information guides subsequent mutagenesis and other experiments to probe the functional relevance of particular structural features, is now well established. As experimental and computational studies of conformational dynamics grow in power and scope, however, the generalization to what might be termed dynamics-function studies has remained challenging. A particular dynamic mode is more difficult to experimentally remove than is, for example, a particular functional group near the active site of an enzyme. These questions

Robert J. Scarborough and Anne Gatignol (eds.), *Ribozymes: Methods and Protocols*, Methods in Molecular Biology, vol. 2167, https://doi.org/10.1007/978-1-0716-0716-9_11,

are of particular interest for ribozymes and other noncoding RNA molecules, for which evidence indicates a particularly prominent role for conformational transitions in molecular function [1–7].

This chapter is concerned with dynamics-function analysis for backbone ribose groups in nucleic acids, for which the most prominent dynamic mode is the interconversion of C3′-endo (A-form) and C2′-endo (B-form) sugar puckers [8, 9]. The correlation of conformational dynamics with function requires two types of analysis: The detection of structural disorder and/or sampling of minor conformations at the atom-specific level, and the assessment of the functional importance of the detected motions. Both of these goals have required methodological advances beyond standard technologies (Fig. 1).

NMR spectroscopic techniques including spin relaxation are powerful methods for the site-specific experimental analysis of dynamics in both proteins and RNA [10–14]. In uniformly ^{13}C-labeled RNA molecules, the standard isotope pattern in samples prepared for NMR spectroscopy, ^{13}C-^{13}C magnetic interactions among the various ribose carbons place severe limits on the applicability of spin-relaxation and related NMR techniques for the analysis of dynamics at those sites. Thus, for valid NMR spin-relaxation analysis of ribose carbon backbone atoms in RNA, ^{13}C isotope labels must be introduced in such a fashion that no one-bond ^{13}C-^{13}C interactions are present [15]. A broadly applicable solution to such limitations is the manipulation of bacterial metabolic pathways in order to place ^{13}C labels at high levels at particular chosen atoms such that all of the directly bonded carbon atoms are the magnetically inert isotope ^{12}C [16–18]. We make use of a metabolic labeling procedure resulting in RNA containing 2′,4′-$^{13}C_2$ nucleotides, providing two appropriate ^{13}C probes per nucleotide. Labeling can be performed for all nucleotides in the molecule or, to help alleviate spectral overlap, for all nucleotides of a particular type (all cytosines, in the example given). We have applied this alternate-site pattern to systems including the GNRA tetraloop [19] and the lead-dependent ribozyme [20].

Functional probing requires the assay of activity (catalysis, ligand binding, or other appropriate parameter) in a molecule containing a mutation or modification specifically quenching the dynamic modes of interest. For RNA ribose groups, for which all naturally occurring nucleotides have identical structures, this is most effectively obtained using chemically modified nucleotides that are covalently restricted to particular regions of the pseudorotation cycle, that is, to particular sugar pucker conformations. In cases where the 2′-hydroxy group is functionally dispensable, this can be done with commercially available locked nucleic acid (LNA) nucleotides [21]. Where the 2′-hydroxyl must be retained, such as at the active site of self-cleaving RNA molecules, more specialized synthetic nucleotides that lock the sugar pucker with retention of

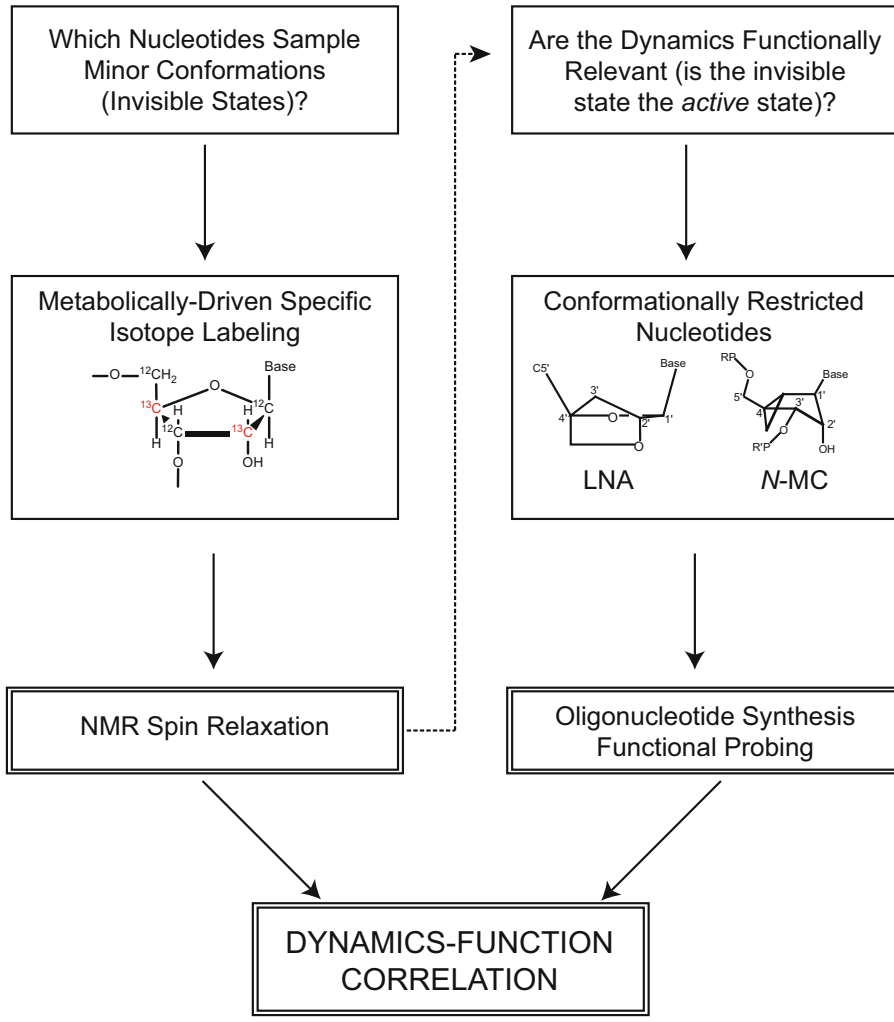

Fig. 1 Schematic view of integrated dynamics-function analysis in noncoding RNA systems. The dashed line indicates that sites of interest for functional probing may in some cases be chosen based on the results of NMR analyses. Double boxes indicate detailed protocols provided in this chapter

the 2′-hydroxyl are required. We describe here the use of synthetic, *North*-locked bicycle[3.1.0]hexane methanocarba (*N*-MC) ribonucleotides [22–26] at the active site of a model ribozyme.

1.1 NMR Studies of Conformational Dynamics: Principles

NMR spin-relaxation and, more recently, chemical exchange saturation transfer (CEST) [27–29] techniques are a rich source of detailed information on conformational dynamics in macromolecules. We describe here the analysis of a single parameter, the ^{13}C transverse relaxation rate measured in the rotating frame ($R_{1\rho}$), which provides a highly informative window into the fundamental properties of the system as well as a foundation for any more detailed analyses [30, 31]. For a hypothetical case in which no internal motion is present, i.e., the molecule is undergoing only

rigid-molecule Brownian tumbling, very similar $R_{1\rho}$ values will be measured for all resonances of a given chemical type (all ^{13}C2′ or ^{13}C4′, for example) (*see* **Note1**). Information on the internal dynamics of the molecule is encoded in $R_{1\rho}$ values that deviate from this globally typical range. For regions of the molecule that display disorder on a sub-nanosecond timescale, transverse relaxation is slower and decreased $R_{1\rho}$ values (longer relaxation times $T_{1\rho}$; *see* **Note 2**) will be observed. By contrast, in the presence of multiple distinct conformations of the molecule that are sampled on timescales of microseconds to milliseconds ("exchange," in NMR parlance), the sampling of states with multiple chemical shifts gives rise to an additional relaxation contribution that can cause $R_{1\rho}$ to be increased (shorter $T_{1\rho}$), sometimes to a dramatic extent.

In a typical $R_{1\rho}$ dataset for a molecule, therefore, a well-defined plateau of very similar values will be observed, corresponding to the rigid framework of the molecule. In nucleic acids, Watson–Crick double helices most typically define that plateau. Individual resonances that show significantly lower $R_{1\rho}$ values then indicate disordered regions of the molecule, whereas significantly increased $R_{1\rho}$ values indicate the presence of multiple conformations, potentially including the sampling of low-probability "invisible states" that are important for molecular function. Example data for ^{13}C2′ and ^{13}C4′ resonances for cytidine resonances in the lead-dependent ribozyme are shown in Fig. 2. Inflated values of $R_{1\rho}$ are observed

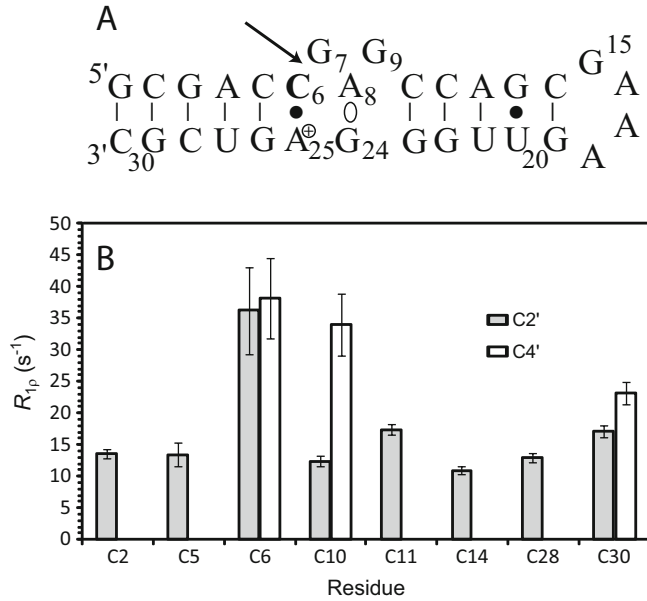

Fig. 2 (**a**) Secondary structure of the lead-dependent ribozyme, indicating the adenosine residue (Ade-25) with a shifted pK_a of 6.5 as positively charged [32], the noncanonical dynamic A-G base pairing interaction (Ade-8◦Gua-24), and the self-cleavage site (arrow). (**b**) Transverse relaxation rates ($R_{1\rho}$) for the 2′,4′-$^{13}C_2$-Cytidine-Leadzyme (Data reproduced from Ref. [20], copyright 2018 Cold Spring Harbor Laboratory Press. Used by permission)

at several sites, notably including the active-site resonance Cyt-6. Since NMR coupling-constant analysis unambiguously indicated the presence of a single major C3′-endo sugar pucker at this site [33], the spin-relaxation results demonstrated the sampling of a low-population C2′-endo state, which was identified with the activated form of the ribozyme [20].

1.2 Scope of This Chapter

Detailed descriptions of methods for the production of isotopically labeled nucleotides from *E. coli* grown in culture and for the incorporation of those nucleotides into defined-sequence RNA via in vitro transcription from synthetic DNA templates have been published and are not reiterated here [34, 35]. For specific isotope labeling using metabolic pathways, identical procedures are followed with the substitution of appropriate bacterial strains and carbon sources. For the 2′,4′-$^{13}C_2$ labeling pattern in this work, a kanamycin-resistant, glucose-6-phosphate negative (*zwf*) *E. coli* strain (JW1841-1, Coli Genetic Stock Center, Yale) was grown on 2-^{13}C-glycerol as the sole carbon source. A wide variety of complementary metabolically driven isotope patterns are available for both amino acids and nucleotides [16, 36]. Similarly, the synthetic route to the *North*-locked ribomethanocarbacytidine phosphoramidite precursor is beyond the scope of this chapter and has been described in detail elsewhere [26]. This protocol describes the modifications to standard solid-phase synthesis necessary to accommodate the modification in the synthesis of the modified ribozyme, as well as subsequent deprotection and purification steps and the assay of self-cleavage activity. The double-outlined boxes in Fig. 1 indicate the stages of a dynamics-function project for which detailed protocols are included herein.

2 Materials

All reagents used should be the highest purity available. Prepare solutions in double-distilled DNase/RNase free molecular biology grade water (ddH_2O).

2.1 NMR Analysis of RNA Dynamics

1. 2-^{13}C-glycerol.
2. *E. coli* strain JW1841-1 (*zwf* genotype, kanamycin-resistant) (Coli Genetic Stock Center, Yale).
3. Standard reagents for molecular biology, sample handling, and large-scale nucleic acid purification.
4. High-resolution NMR spectrometer operating at 500 MHz ^{1}H frequency or greater with variable temperature control, pulsed field gradient unit, and a ^{1}H-detect probe with at least one broadband decoupler channel (*see* **Note 3**).

5. Linux computer with NMRPipe, NMRDraw, and Sparky or NMRFAM-Sparky software packages installed (*see* **Note 4).**

2.2 Modified Ribozyme Kinetic Analysis

2.2.1 Solid-Phase RNA Synthesis

1. Phosphoramidite of the *North* pseudosugar modification (*N*-methanocarba derivative) of the desired nucleotide containing a 2′-*O*-(2-cyanoethoxymethyl) (CEM) protecting group. The synthetic procedure is described in detail by Terrazas et al. [26].
2. Unmodified nucleotide precursors: 5′-*O*-(4,4-′-dimethoxytrityl)-2′-*O*-*tert*-butyldimethylsilyl-3′-*O*-(2-cyanoethyl)-*N*,*N*-diisopropyl phosphoramidites: N^2-dimethylformamidine-guanosine (dmf-G-CE phosphoramidite); N^6-Benzoyl-adenosine (Bz-A-CE phosphoramidite); Uridine (U-CE phosphoramidite); N^4-Benzoyl-cytidine (Bz-C-CE phosphoramidite).
3. Substrate: RNA controlled-pore glass (CPG) DMT-C-support.
4. Fluorophore label: 5′-fluorescein-CE phosphoramidite of the 5′-terminal nucleotide.
5. Solid-phase RNA synthesis reagents: Acetic anhydride in THF/pyridine; 16% 1-methylimidazole in THF; 0.02 M iodine in THF/pyridine/water; 1H-tetrazole in anhydrous acetonitrile; 3% trichloroacetic acid in CH_2Cl_2; Anhydrous CH_2Cl_2; Anhydrous acetonitrile; 10% *t*-butylhydroperoxide in acetonitrile/water (96:4); 0.01 M iodine in tetrahydrofuran/pyridine/water (7:2:1).
6. Instrumentation: DNA synthesizer (*e.g.*, Applied Biosystems Model 3400); Argon source; HPLC column Nucleosil 120 C18 (250 × 8 mm); Heating block; SpeedVac concentrator; Hamilton gas-tight syringe; 3-mL glass vials.

2.2.2 RNA Deprotection and Purification

1. Deprotection reagents: Concentrated ammonia, ethanol, *n*-propylamine, bis(2-mercaptoethyl) ether; tetra-*n*-butylammonium fluoride (TBAF); triethylammonium acetate (TEAA); NAP-5 or similar desalting column.
2. Reversed-phase chromatography solutions: A, 5% CH_3CN in 100 mM triethylammonium acetate (TEAA) pH 6.5; B, 70% CH_3CN in 100 mM TEAA pH 6.5.

2.2.3 Ribozyme Activity Assay

1. MOPS, or appropriate buffer for the activity assay of interest.
2. $Pb(OAc)_2$, freshly prepared stock solution.
3. Stock solutions for denaturing PAGE: 5× TBE, 40% 19:1 acrylamide:bisacrylamide, 10 M urea [37].
4. Fluorescence gel quantitation system (Bio-Rad Fluor-S MAX MultiImager or similar).

3 Methods

3.1 NMR Analysis of Ribose Dynamics

3.1.1 NMR Data Acquisition

1. Prepare the specifically isotope-labeled NMR sample according to published procedures (*see* Subheading 1). For the 2′,4′-$^{13}C_2$ nucleotide labeling pattern, use the JW1841–1 (*zwf* genotype, kanamycin-resistant) strain of *E. coli* and grow the bacteria on 2-^{13}C-glycerol as the sole carbon source. Perform in vitro transcription using the resulting specifically labeled nucleotide (s) for nucleotide type(s) of interest and unlabeled nucleotides for all others. Purify the sample on a size exclusion column [35, 38] and dialyze extensively into the final buffer (*see* **Note 5**).
2. Anneal the sample in the NMR tube at 85 °C for 2 min followed by slow cooling to room temperature (*see* **Note 6**).
3. Insert the NMR sample into the magnet, tune the ^{1}H and ^{13}C channels, and shim the field to homogeneity (*see* **Note 7**).
4. From the VnmrJ "Experiments" menu, run the setup macro for the RNA/DNA two-dimensional ^{1}H/^{13}C HSQC. This will load the basic parameters for the experiment along with the standard amplifier powers and pulse widths according to the probefile maintained by the NMR system administrator.
5. Optionally, calibrate the 90° pulse widths. If the probefile is accurate, the default pulse widths should be close to optimal, but this procedure will optimize sensitivity and identify any problems with system configuration. Set the pulse sequence to 1D mode (phase = 0, ni = 0). Acquire a 1D spectrum, phase, and expand the region of interest. For ^{1}H, set the calH parameter to an array of three values, calH = 1.8, 2, 2.2. Increase nt to at least 128 to achieve sufficient signal to noise at close to the null. Acquire data and display the results as a horizontal array ("wft dssh"). If the pulse width is accurate, the first spectrum should be of small magnitude and positive, the second should be null with possibly some residual dispersive intensity, and the third should be of the same magnitude as the first but negative. If this is not the case, adjust "pw" until this pattern is seen, and use that pw for the acquisition. Return calH = 1.0. For ^{13}C, repeat this procedure, using calC to optimize pwC.
6. If desired, acquire a standard HSQC spectrum for reference using the default parameters.
7. Adjust the acquisition for relaxation measurements by choosing the "C13 T1rho" and "ribose" radio buttons under the Acquire>Pulse Sequence tab. Set the remaining acquisition parameters according to Table 1 (Table 1 gives both the parameter descriptions shown in the GUI and the Vnmr parameter names for entry at the command line).

Table 1
VnmrJ parameters for acquisition of ^{13}C $R_{1\rho}$ data on $^{13}C2'$ and $^{13}C4'$ resonances

Parameter label from GUI	VnmrJ parameter name	Value
Acquisition tab		
^{1}H Sweep Width (Hz)	sw	2400
Data size	np	1024 (*see* **Note 23**)
Number of scans	nt	See main text
Steady-state scans	ss	64
Relaxation delay	d1	1 sec
Observe pulse width	pw	Set by probefile
Pulse power	tpwr	Set by probefile
Decoupler pulse width	pwC	Set by probefile
Decoupler pulse power	pwClvl	Set by probefile
^{13}C spectral width	sw1	14 ppm (2100 Hz)
Number of increments	ni	80
Acquisition mode	phase	Hypercomplex 2D (phase = 1,2)
Half-dwell delay in t_1	f1180	on (y)
Pulse sequence tab		
N15 refocus in t_1	N15refoc	off (n)
Mode radio button: ribose	ribose aromatic allC	on (y) off (n) off (n)
Observe only CH2s	CH2only	off (n)
F1 detection mode radio button	Sensitivity-enhanced	SE = "y" (*see* **Note 24**) ZZ = "n"
Relaxation radio button	T1rho	On (y)
Mixing time	relaxT	See main text
Maximum mix time	maxrelaxT	See main text
J(13C-1H)	JCH	145 (*see* **Note 25**)
Refocusing time	tCH	0.00172
Constant time	CT	off (n)
Channels tab		
1H Offset	tof	Set to HDO resonance
13C Offset	dof	104 ppm (*see* **Notes 26** and **27**)
Decoupler mode	dm	nny
Decoupler modulation mode	dmm	ccp
Decoupler sequence	dseq	wurst80

8. Set the relaxation time relaxT to one of the shorter relaxation times to be acquired, in seconds (e.g., relaxT = 0.010 for 10 ms). Set maxrelaxT to the longest relaxation time to be used, also in seconds (*see* **Note 8**).
9. Set the number of transients (nt) to a multiple of the phase cycle length (8 for "rna_gChsqc") sufficient to achieve good signal to noise, remembering that signal intensity will decrease substantially for longer relaxT time points. The exact value needed will depend on sample concentration, molecular size, available time, and other factors. We generally find that an experimental duration of between two and four hours provides reasonable results for typical samples.
10. Copy the final parameters to the desired number of other experimental workspaces ("exp" values, in Vnmr). In each of those workspaces, adjust only the relaxT parameter. In general, between 8 and 12 values of relaxT, with several falling both shorter and longer than the expected $R_{1\rho}$ values, will define the rates well. Variation between 0 ms and 120 ms is sufficient for typical systems (*see* **Note 9**). relaxT must be set to a multiple of 5 ms. Short and long relaxT values must be distributed randomly rather than in simple descending or ascending order to prevent errors in measured rates arising from instrumental or sample instability. Repeat one relaxT value (we often use 10 ms) at least three times to allow error analysis, interspersed throughout the series.
11. Acquire data in one uninterrupted series, i.e., without removing the sample from the magnet, adjusting the tuning or shimming, or filling cryogens. Save each dataset to disk and, if not to be analyzed directly on the spectrometer console, transfer to the offline workstation for processing and analysis.

3.1.2 Data Format Conversion

1. Processing should be performed on a Linux computer with NMRPipe, NMRDraw, and Sparky or NMRFAM-Sparky [39, 40] installed (*see* **Note 4**). Consult with the local system administrator for proper installation and configuration of these packages and associated utilities.
2. In a unix shell window, use the command "varian" to invoke a graphical user interface (GUI) for file conversion.
3. Click the green arrow (Spectrometer Input) to select the appropriate time-domain free induction decay (fid) file.
4. Click "Read Parameters." The parameters in the GUI should now reflect the input data. If the NMR data was obtained in sensitivity-enhanced mode (SE = "y"), use the "Rance-Kay" option for the indirect dimension. Otherwise (SE = "n," ZZ = "y"), select "Complex" (*see* **Note 10**).

A

```
#!/bin/csh
var2pipe  -in ./fid

-noaswap

 -xN   1024                    -yN          160
 -xT   512                     -yT          80
 -xMODE          Complex       -yMODE           Rance-Kay
 -xSW          2400.240        -ySW             2111.741
 -xOBS          599.732        -yOBS            150.827
 -xCAR            4.773        -yCAR            104.163
 -xLAB             1H  -       yLAB             C13
 -ndim               2          -aq2D            Complex

 -out ./test.fid -verb -ov
```

B

```
#!/bin/csh
#
# Basic 2D Phase-Sensitive Processing:
#
#   Use of "ZF -auto" doubles size, then rounds to power of 2.
#   Use of "FT -auto" chooses correct Transform mode.
#   Imaginaries are deleted with "-di" in each dimension.
#   Phase corrections should be inserted by hand.

nmrPipe -in test.fid
| nmrPipe  -fn EM  -lb 8.0 -c 1.0                #window function in t2
| nmrPipe  -fn ZF -auto
| nmrPipe  -fn FT -auto
| nmrPipe  -fn PS -p0 247.4 -p1 -1.6 -di -verb   #phases set empirically
| nmrPipe  -fn TP -auto
| nmrPipe  -fn LP -pred 48
| nmrPipe  -fn SP -off 0.5 -end 1.0 -pow 2       #window function in t1
| nmrPipe  -fn ZF -auto
| nmrPipe  -fn FT -auto
| nmrPipe  -fn PS -p0 -90 -p1 180 -di -verb      #appropriate half-dwell phases
| nmrPipe  -fn TP -auto
  -ov -out test.ft2
```

Fig. 3 Example Linux shell scripts for data handling. (**a**) Format conversion from Varian/Agilent to NMRPipe-compatible raw data. (**b**) Two-dimensional Fourier transformation

5. Click “Save Script.” By default, this creates a file “fid.com” in the home folder. The name or destination can be changed if desired, but it often smoothes the workflow in later steps to use the default. A typical shell script invoking the “var2pipe” utility is shown in Fig. 3a.

6. Click "Execute Script." A reformatted "test.fid" file will be generated. If the default filenames have been used, rename and move the .com and .fid files into a separate folder, as they will otherwise be overwritten by the next file conversion.
7. Repeat the file conversion for each dataset.

3.1.3 Data Processing and Visualization

1. Choose a single spectrum at relatively short relaxation delay to develop and optimize processing. Open the corresponding test.fid file with NMRDraw. All dimensions should be in units of time at this point. The following steps will perform a two-dimensional Fourier transformation yielding an HSQC-type spectrum with two frequency axes (*see* **Note 11**).
2. If a previously used NMRPipe processing script is not available as a template, use "macro edit" (File menu) in NMRDraw to generate one. For initial processing, use pre-formulated processing schemes, i.e., Process-2D and then Basic-2D. Save and move the script file (by default, "nmrproc.com") to the folder with previous files (*see* **Note 12**). A model processing script is shown in Fig. 3b (*see* **Note 13**).
3. Close NMRDraw "shft+q."
4. Copy and paste the nmrproc.com file to folder with previously generated files.
5. Execute the nmrproc.com file (*see* **Note 14**).
6. Open ft2.test with NMRDraw.
7. Inspect the processed result and phase by hand (*see* **Note 15**).
8. Process each spectrum using identical versions of the processing macro. This can be done by making copies of the macro with the input and output filenames changed.

3.1.4 Relaxation Analysis

1. Convert the NMRPipe files to Sparky format. Use the following example command as a template:
   pipe2ucsf rho120.pipe rho120.ucsf.

   This command converts the processed data file rho120.pipe (equivalent to ft2.test in the above example) into the Sparky-readable output file rho120.ucsf. It is efficient to put the relaxation time in the output filename as shown (120 ms in this example) because Sparky will be able to automatically detect it later (*see* **Note 16**).
2. Create a folder in "Projects" in the Sparky directory for the files.
3. Assign peaks in one spectrum and copy and paste the assignments through to all spectra (*see* **Note 17**).
4. Extract relaxation rates for each peak in the dataset using the rh command (*see* **Note 18**).

3.2 Modified Ribozyme Kinetic Analysis

3.2.1 Solid-Phase RNA Synthesis (See **Note 19**)

1. Dissolve 0.1 mmol of *North*-ribomethanocarba phosphoramidite for the nucleotide of interest in anhydrous acetonitrile to obtain a 0.1 M solution in a 10-mL synthesizer vial capped with a rubber septum using a gas-tight syringe. Load the vial in the synthesizer using the change bottle protocol.
2. Load the remaining phosphoramidites including the 5′-fluorescein-CE phosphoramidite and the rest of the RNA synthesis reagents into the synthesizer. Mount an RNA synthesis column with 1 μmol of RNA controlled-pore glass (CPG) support corresponding to the first nucleoside at the 3′-end of the RNA sequence onto the synthesis port of the synthesizer.
3. Perform the automated solid-phase assembly of the oligonucleotide from the 3′ terminus through the nucleotide immediately 3′ to the modification site using DMT-off protocols. Use standard 0.01 M iodine in tetrahydrofuran/pyridine/water (7:2:1) as the oxidizer and a 15 min coupling time.
4. Incorporate the *North* pseudosugar modification (C^*) using the corresponding phosphoramidite derivative. Next, incorporate the remaining natural nucleotide units using the same procedure as the first part, with the exception of the oxidation solution. In order to avoid cleavage at the modification site [23], use 10% *t*-butylhydroperoxide in acetonitrile/water (96:4) as the oxidizing solution in these steps, replacing the iodine solution used in the previous steps. Use a 15 min phosphoramidite coupling time at all steps. Yield should exceed 90% for the modified-nucleotide step and 98% for all other steps.
5. Incorporate the fluorescein label at the 5′-end of the strand using 5′-fluorescein-CE phosphoramidite. Coupling time: 5 min.
6. Remove the column from the synthesizer and dry the column with a stream of argon or nitrogen.
7. Transfer the CPG-oligonucleotide support to a 3-mL vial, add 1.5 mL of concentrated aqueous ammonia and 0.5 mL of ethanol, and incubate the vial at 55 °C for 1 h.
8. Cool the vial on ice and transfer the supernatant into a 2 mL Eppendorf tube.
9. Rinse the solid support and the vial with 50% ethanol (2 × 0.25 mL).
10. Evaporate the combined solutions to dryness using an evaporating centrifuge (*see* **Note 20**).

3.2.2 Ribozyme 2′-Deprotection and Purification

1. Dissolve the residue from Subheading 3.2.1, **step 10** in a mixture formed by 10 μL of n-propylamine, 1 μL of bis (2-mercaptoethyl) ether, and 100 μL of 1 M TBAF in THF and rock at room temperature for 24 h.

2. Add 100 μL of 1 M triethylammonium acetate (TEAA) and 289 μL of water to the solution.
3. Desalt the oligonucleotide on a NAP-5 column using water as the eluent and evaporate to dryness.
4. Purify the sample by reversed-phase high performance liquid chromatography (RP-HPLC) using a Nucleosil 120 or comparable C18 column eluted at a flow rate of 3 mL/min with a 20 min linear gradient from 0% to 50% B and 5 min isocratic at 50% B.
5. Pool the fractions containing the desired oligonucleotide, concentrate the solution using a SpeedVac concentrator, and desalt by passing through a Sephadex NAP-25 column.
6. Analyze the molecular weight by mass spectrometry (MALDI-ToF) for quality control.

3.2.3 Ribozyme Activity Assay

1. Procedures are given here for activity assays in the self-cleaving lead-dependent ribozyme system. For other ribozymes such as the Mg^{2+}-activated hammerhead or hairpin motifs, these procedures will vary in the use of activating metal ion and in the details of assay procedures, and the literature in the appropriate system should be consulted. For functional analysis of RNAs of different classes (self-splicing ribozymes, riboswitches, aptamers binding small molecules or proteins, etc.), assays appropriate to the system will of course be used, but the synthesis and handling of *N*-MC modified RNA molecules will be as described in Subheadings 3.2.1 and 3.2.2.
2. Using Amicon Ultra-15 centrifugal filtration units, exchange the synthesized RNAs against ddH_2O at least three times followed by exchange into 15 mM MOPS Buffer (pH 7.0) (*see* **Note 5**).
3. Verify the RNA purity using denaturing polyacrylamide electrophoresis with a gel composition of 20% 19:1 polyacrylamide:bispolyacrylamide, 7 M urea, 1× TBE. Run the gel at 150 V with a one-hour pre-run, typical run time 40 minutes. Visualize the gel using UV shadowing on a fluorescent TLC plate with a hand-held ultraviolet lamp or a gel documentation system. RNA should run as a single band of appropriate size.
4. Determine RNA concentrations using ultraviolet spectrophotometry at 260 nm. For the leadzyme, the single-stranded extinction coefficient (ε) is $2.95 \times 10^5\ M^{-1}\ cm^{-1}$ for both unmodified and modified RNAs (*see* **Note 21**).
5. Perform **steps 6** through **14** in parallel with modified and unmodified RNA sequences.
6. Renature RNA samples via heating at 85 °C for 2 min and allow them to cool slowly to room temperature (*see* **Note 6**).

7. Prepare fresh stock 50 μM $Pb(OAc)_2$, 15 mM MOPS solution (*see* **Note 22**).
8. In an ultracentrifuge tube, mix sufficient RNA stock to bring the 50 μL reaction mixture to 1 μM RNA with sufficient 15 mM MOPS (pH 7.0) buffer to reach 50 μL once Pb(II) is added. For leadzyme kinetics, typical target concentrations of $Pb(OAc)_2$ are 10, 25, 50, 100, 200, and 300 μM. Higher concentrations may be omitted if needed as they are typically beyond the point where the poor solution behavior of Pb(II) at neutral pH leads to decreasing activity.
9. Equilibrate the buffered RNA and freshly made $Pb(OAc)_2$ stock solution at the assay temperature (27 °C) for 15 min.
10. Initiate the cleavage reaction by the addition of $Pb(OAc)_2$ to the appropriate final concentration. Mix briefly. Return to the equilibration bath.
11. At time points of 20 s (or as soon as can be reproducibly obtained with manual pipetting), 1, 5, 15, 30, 60, 120, and 180 min, remove a 5 μL aliquot of the reaction mixture for analysis.
12. Immediately quench each aliquot via addition to 5 μL of a 9 M urea/50 mM EDTA mixture followed by freezing on dry ice.
13. Analyze the cleavage reactions via denaturing 20% polyacrylamide gels as in **step 3** above. Visualize using a Bio-Rad Fluor-S MAX MultiImager or similar instrument with fluorescence excitation at 494 nm and detection at 518 nm.
14. Quantitate substrate and 5′-cleavage product gel bands and background signals using software supplied by the manufacturer (e.g., Bio-Rad Quantity One). Subtract background intensity from all band intensities. Calculate the percentage of cleavage product as (product/[product + substrate]) at each time point.
15. Determine the exponential decay rate for the data via nonlinear fitting in a standard data analysis software package (e.g., Origin, SigmaPlot, Igor Pro) or spreadsheet. Manual inspection of the fits and residuals is critical since catalytic RNA constructs often give rise to multiexponential behavior, attributed to a misfolded or degraded fraction of the ribozyme. In this case, fit the data to a double-exponential function and report the faster-cleaving fraction for functional comparisons. If the single- versus double-exponential character of the data is ambiguous, assess the statistical significance of the improvement in the fit using standard statistical techniques such as the "F" test [41].

4 Notes

1. Dramatic deviations of the molecule from isotropic (spherically symmetric) overall tumbling can also cause variations in relaxation parameters, albeit generally of smaller magnitude than those observed here. If the structure of the molecule is known, these effects may be taken into account with a more sophisticated computational analysis than is described here [30, 42].
2. NMR relaxation experiments may be reported as either relaxation rates or relaxation times, related as simple reciprocals (e.g., $T_{1\rho} = 1/R_{1\rho}$). Since both terms are in common use, care must be taken to avoid confusion in interpretation.
3. We have successfully performed relaxation experiments at fields ranging from 500 to 900 MHz (125–225 MHz in ^{13}C) [3, 19, 20, 43]. In addition to achieving adequate sensitivity and resolution for the sample of interest, the key consideration in the choice of field used is that the exchange contributions to transverse relaxation (R_{ex}) that are of fundamental interest here scale as the square of the static field. Relatively weak effects may be undetectable at lower fields; conversely, very strong R_{ex} contributions may lead to sufficiently fast relaxation that the curve cannot be analyzed, or the NMR peak itself may broaden to undetectability [19]. Acquisition of pilot data at multiple static fields may be of use to determine the optimum field strength.
4. Links to the most current versions of these and many other NMR software routines are maintained by the National Center for Biomolecular NMR Data Processing and Analysis at http://www.nmrbox.com.
5. RNA is a polyanion, and solutions of RNA molecules, especially at biophysical and spectroscopic concentrations, are therefore prone to counterion condensation effects that deplete cations from bulk solution and can lead to irregular results if RNA is simply brought up in a buffer of a given ionic strength. It is critical for RNA stocks to be prepared via extensive dialysis against the desired buffer in order to define the correct bulk-solution ion concentrations. We commonly achieve this using repeated dilution cycles into the desired buffer using Amicon-type centrifugal concentrators. To optimize sample recovery, two concentrators can be used in a sequential fashion, i.e., the flow-through of the first unit can be used as input to a second unit. The final retentates of the two units are then combined to yield the stock solution.
6. Annealing protocols designed to bring RNA preparations with different thermal histories to a consistent conformational state are developed empirically for each RNA construct and can vary

widely. In the absence of stabilizing elements such as the GAAA tetraloop, best results may be obtained in the absence of any annealing steps at all. The literature in the system of interest should be consulted and sample-handling protocols scrupulously followed in order to obtain consistent results.

7. Procedures for instrument tuning and adjustment should follow the documentation for the particular system in use. For experimental setup, spectrometers from different manufacturers and to some extent different software versions will use different command and parameter names to accomplish very similar tasks. We describe here instrument setup at 600 MHz using VnmrJ 3.2A on a Varian (now Agilent) spectrometer with pulse programs from Varian BioPack/RNAPack [44]. Setup on other systems can be done in largely parallel fashion.
8. The maxrelaxT parameter is designed to compensate for any errors introduced by heating of the sample arising from the ^{13}C spin lock pulse. It applies irradiation for a period of (maxrelaxT − relaxT) prior to each execution of the pulse sequence, resulting in a constant RF power deposition in the sample for all values of relaxT.
9. In general, a zero-time point will yield distorted results due to off-axis magnetization that is dephased during the first few millisecond of the spin lock. The Biopack rna_gChsqc pulse sequence, however, hardwires a 5 ms delay preceding relaxT, and a relaxT = 0.0 point is therefore useful.
10. Either at this point or following transformation, the ^{13}C carrier frequency should be adjusted from 104 to 79 ppm to account for the effects of the Biopack pulse sequences (*see* Table 1, **Note 26**).
11. When calling NMRPipe routines from its graphical interface, NMRDraw uses virtual memory rather than saving every processing step to disk. This is useful for development and debugging, but the final script should be re-executed from the command line to ensure that data is retained for downstream analysis.
12. Detailed documentation of NMRPipe is available at the developer's website, http://spin.niddk.nih.gov/NMRPipe/doc1/, currently supported at https://www.ibbr.umd.edu/nmrpipe/index.html. Commands found in processing scripts are documented in full at http://www.nmrscience.com/ref/index.html.
13. The choice of window functions to be applied to the data in each dimension can substantially affect the properties of the processed data. We typically use an exponential multiplication window in the directly detected dimension, with a line

broadening of between 4 and 12 Hz depending on the dataset (in Fig. 3b, EM –lb 8.0 gives an 8 Hz broadening). Stronger windows (higher broadening values) improve the signal to noise of the spectrum at the cost of worsening spectral overlap between neighboring peaks. In the indirect dimension, a cosine (in Fig. 3b, SP –off 0.5) or cosine-squared window generally gives good results. It is critical that identical processing parameters be used for each spectrum in a single relaxation dataset.

14. Running the nmrproc.com script from the command line in a terminal window, rather than double clicking it in the LINUX GUI, provides a readout of the progress as the file is being processed. This is very helpful in identifying the specific component of the processing script that is leading to execution errors or other problems.
15. Phase parameters must be adjusted manually by examination of the transformed spectrum. The phase values (PS) are adjusted in gedit or another text editor and nmrproc.com is then re-executed. If f1180 is set to "y," the phasing in the indirect dimension should be very close to $p0 = +90$, $p1 = -180$ for SE = "n" and $p0 = -90$, $p1 = +180$ for SE = "y." Once phase parameters are optimized on the test spectrum, identical values of $p0$ and $p1$ should be used for all spectra in the relaxation series.
16. For converting NMRPipe-processed spectra to Sparky compatible files, refer to the following link: https://www.cgl.ucsf.edu/home/sparky/manual/files.html#ConvertNMRPipe.
17. The process of assigning individual peaks and copying and pasting the assignments is documented in the manual for Sparky, https://www.cgl.ucsf.edu/home/sparky/manual/peaks.html.
18. Performing relaxation analysis using the rh command is documented in the Sparky manual, https://www.cgl.ucsf.edu/home/sparky/manual/extensions.html#RelaxFit.
19. For commercially available locked nucleic acid nucleotides, standard oligo synthesis performed by the vendor or other available facilities may be used.
20. Long-term storage and (if necessary) shipping of RNA should be at this step, prior to 2′-deprotection. Overnight shipping can be performed in tightly sealed containers at room temperature, but storage should be at −20 °C or below. Following 2′-deprotection, RNA should always be maintained at −20 °C or below and handled on ice or in a cold chamber.
21. Extinction coefficients calculated using standard nearest-neighbor approaches will be slightly different for the modified nucleotide-containing sequence, but this difference is of no

functional consequence for the present purpose. For example, the presence of five pseudouridine modifications was found to lead to no experimentally detectable change in the extinction coefficient of a 19-nucleotide oligo (M.S., unpublished results). If precise concentrations are needed, the experimental extinction coefficient can be determined via RNA digestion with P1 nuclease [45].

22. The use of freshly prepared $Pb(OAc)_2$ solutions is critical for reliable results.
23. NMR data are reported in complex (pairs of real and imaginary) points. In VnmrJ, an "np" value of 1024 yields 512 complex points in the acquisition (^{1}H) dimension. In contrast, an "ni" value of 80 yields 80 complex points in the indirectly acquired (^{13}C) dimension. Care should be taken to ensure that the parameters used by the processing software correspond to these conventions.
24. The "SE" option invokes sensitivity-enhanced pulse sequence elements that retain complementary coherence transfer pathways [46]. These often yield improved results, but when used in larger molecules these advantages may disappear or reverse owing to the increased numbers of pulses and delays. If in doubt, a comparison of the signal obtained for the first slice of an HSQC (ni = 0, phase = 1) for ZZ = "n"/SE = "y" versus ZZ = "y"/SE = "n" will indicate the optimal setup.
25. Due to an error in the VnmrJ3.2A macros, changing the "J (13C-1H)" parameter in the GUI does not affect the actual value of the JCH parameter used for acquisition. This parameter should always be adjusted and verified at the command line.
26. The Biopack pulse sequences installed on many Varian/Agilent spectrometers assume that the ^{13}C carrier is always set by the user to 110 ppm, and the pulse programs then adjust the carrier to the appropriate chemical shift for a given experiment. The rna_gChsqc pulse sequence with the ribose = "y" flag set subtracts 25 ppm from the preset carrier to yield a spectrum centered at 85 ppm. For 2′,4′-$^{13}C_2$ samples, however, the optimal carrier setting is ca. 79 ppm, midway between the ^{13}C2′ and ^{13}C4′ resonances. The user should thus set the carrier to the fictitious value of 104 ppm, which the pulse sequence will then adjust to 79 ppm.
27. At ultrahigh static magnetic field strengths, it may be advantageous to acquire separate datasets for ^{13}C2′ and ^{13}C4′ resonances, with the carrier placed at the center of each spectral region, in order to avoid effects from resonance offset [19].

Acknowledgments

The authors are grateful to Dr. Victor Marquez and Dr. Ramon Eritja for helpful discussions and the U.S. National Science Foundation (MCB-1413356 to C.G.H.) and the Spanish Ministry of Economy (MINECO) (CTQ2017-84415-R to Ramon Eritja) for funding support.

References

1. Hoogstraten CG, Sumita M (2007) Structure-function relationships in RNA and RNP enzymes: Recent advances. Biopolymers 87:317–328
2. Lee TS, Radak BK, Harris ME et al (2016) A two-metal-ion-mediated conformational switching pathway for HDV ribozyme activation. ACS Catal 6:1853–1869
3. Legault P, Hoogstraten CG, Metlitzky E et al (1998) Order, dynamics, and metal binding in the lead-dependent ribozyme. J Mol Biol 284:325–335
4. Lemieux S, Chartrand P, Cedergren R et al (1998) Modeling active RNA structures using the intersection of conformational space: application to the lead-activated ribozyme. RNA 4:739–749
5. Martick M, Scott WG (2006) Tertiary contacts distant from the active site prime a ribozyme for catalysis. Cell 126:309–320
6. Murray JB, Dunham CM, Scott WG (2002) A pH-dependent conformational change, rather than the chemical step, appears to be rate-limiting in the hammerhead ribozyme cleavage reaction. J Mol Biol 315:121–130
7. Yajima R, Proctor DJ, Kierzek R et al (2007) A conformationally restricted guanosine analog reveals the catalytic relevance of three structures of an RNA enzyme. Chem Biol 14:23–30
8. Altona C, Sundaralingam M (1972) Conformational analysis of the sugar ring in nucleosides and nucleotides. A new description using the concept of pseudorotation. J Am Chem Soc 94:8205–8212
9. Wijmenga SS, Van Buuren BNM (1998) The use of NMR methods for conformational studies of nucleic acids. Prog Nucl Magn Reson Spectrosc 32:287–387
10. Al Hashimi HM, Walter NG (2008) RNA dynamics: it is about time. Curr Opin Struct Biol 18:321–329
11. Bothe JR, Nikolova EN, Eichhorn CD et al (2011) Characterizing RNA dynamics at atomic resolution using solution-state NMR spectroscopy. Nat Methods 8:919–931
12. Dethoff EA, Petzold K, Chugh J et al (2012) Visualizing transient low-populated structures of RNA. Nature 491:724–728
13. Furtig B, Buck J, Richter C et al (2012) Functional dynamics of RNA ribozymes studied by NMR spectroscopy. Methods Mol Biol 848:185–199
14. Latham MP, Brown DJ, Mccallum SA et al (2005) NMR methods for studying the structure and dynamics of RNA. Chembiochem 6:1492–1505
15. Johnson JE Jr, Julien KR, Hoogstraten CG (2006) Alternate-site isotopic labeling of ribonucleotides for NMR studies of ribose conformational dynamics in RNA. J Biomol NMR 35:261–274
16. Hoogstraten CG, Johnson JE Jr (2008) Metabolic labeling: taking advantage of bacterial pathways to prepare spectroscopically useful isotope patterns in proteins and nucleic acids. Concepts Magn Resonan A 32:34–55
17. Leblanc RM, Longhini AP, Tugarinov V et al (2018) NMR probing of invisible excited states using selectively labeled RNAs. J Biomol NMR 71:165–172
18. Longhini AP, Leblanc RM, Becette O et al (2016) Chemo-enzymatic synthesis of site-specific isotopically labeled nucleotides for use in NMR resonance assignment, dynamics and structural characterizations. Nucl Acids Res 44: e52
19. Johnson JE Jr, Hoogstraten CG (2008) Extensive backbone dynamics in the GCAA RNA tetraloop analyzed using ^{13}C NMR spin relaxation and specific isotope labeling. J Am Chem Soc 130:16757–16769
20. White NA, Sumita M, Marquez VE et al (2018) Coupling between conformational dynamics and catalytic function at the active site of the lead-dependent ribozyme. RNA 24:1542–1554
21. Julien KR, Sumita M, Chen P-H et al (2008) Conformationally restricted nucleotides as a probe of structure-function relationships in RNA. RNA 14:1632–1643

22. Ketkar A, Zafar MK, Banerjee S et al (2012) A nucleotide-analogue-induced gain of function corrects the error-prone nature of human DNA polymerase iota. J Am Chem Soc 134:10698–10705
23. Maier MA, Choi Y, Gaus H et al (2004) Synthesis and characterization of oligonucleotides containing conformationally constrained bicyclo[3.1.0]hexane pseudosugar analogs. Nucleic Acids Res 32:3642–3650
24. Marquez VE, Ezzitouni A, Siddiqui MA et al (1997) Conformational analysis of nucleosides constructed on a bicyclo[3.1.0]hexane template. Structure-antiviral activity analysis for the northern and southern hemispheres of the pseudorotational cycle. Nucleosides Nucleotides 16:1431–1434
25. Saneyoshi H, Mazzini S, Avino A et al (2009) Conformationally rigid nucleoside probes help understand the role of sugar pucker and nucleobase orientation in the thrombin-binding aptamer. Nucleic Acids Res 37:5589–5601
26. Terrazas M, Avino A, Siddiqui MA et al (2011) A direct, efficient method for the preparation of siRNAs containing ribo-like North bicyclo [3.1.0]hexane pseudosugars. Org Lett 13:2888–2891
27. Vallurupalli P, Bouvignies G, Kay LE (2012) Studying "invisible" excited protein states in slow exchange with a major state conformation. J Am Chem Soc 134:8148–8161
28. Zhao B, Hansen AL, Zhang Q (2014) Characterizing slow chemical exchange in nucleic acids by carbon CEST and low spin-lock field R(1rho) NMR spectroscopy. J Am Chem Soc 136:20–23
29. Zhao B, Zhang Q (2015) Measuring residual dipolar couplings in excited conformational states of nucleic acids by CEST NMR spectroscopy. J Am Chem Soc 137:13480–13483
30. Palmer AG III (2004) NMR characterization of the dynamics of biomacromolecules. Chem Rev 104:3623–3640
31. Palmer AG III, Massi F (2006) Characterization of the dynamics of biomacromolecules using rotating-frame spin relaxation NMR spectroscopy. Chem Rev 106:1700–1719
32. Legault P, Pardi A (1997) Unusual dynamics and pK_a shift at the active site of a lead-dependent ribozyme. J Am Chem Soc 119:6621–6628
33. Hoogstraten CG, Legault P, Pardi A (1998) NMR solution structure of the lead-dependent ribozyme: evidence for dynamics in RNA catalysis. J Mol Biol 284:337–350
34. Batey RT, Battiste JL, Williamson JR (1995) Preparation of isotopically enriched RNAs for heteronuclear NMR. Methods Enzymol 261:300–322
35. Mckenna SA, Kim I, Puglisi EV et al (2007) Purification and characterization of transcribed RNAs using gel filtration chromatography. Nat Protoc 2:3270–3277
36. Longhini AP, Leblanc RM, Dayie TK (2016) Chemo-enzymatic labeling for rapid assignment of RNA molecules. Methods 103:11–17
37. Green MRS, J. (2012) Molecular cloning: a laboratory manual. Cold Spring Harbor Laboratory Press, Cold Spring Harbor, NY
38. Kim I, Mckenna SA, Viani PE et al (2007) Rapid purification of RNAs using fast performance liquid chromatography (FPLC). RNA 13:289–294
39. Delaglio F, Grzesiek S, Vuister GW et al (1995) NMRPipe: a multidimensional spectral processing system based on UNIX pipes. J Biomol NMR 6:277–293
40. Lee W, Tonelli M, Markley JL (2015) NMRFAM-SPARKY: enhanced software for biomolecular NMR spectroscopy. Bioinformatics 31:1325–1327
41. Bevington PR, Robinson DK (2003) Data reduction and error analysis for the physical sciences, 3rd edn. McGraw-Hill, New York, NY
42. Kay LE, Torchia DA, Bax A (1989) Backbone dynamics of proteins as studied by ^{15}N inverse detected heteronuclear NMR spectroscopy: application to staphylococcal nuclease. Biochemistry 28:8972–8979
43. Hoogstraten CG, Wank JR, Pardi A (2000) Active site dynamics in the lead-dependent ribozyme. Biochemistry 39:9951–9958
44. Lukavsky PJ, Puglisi JD (2001) RNAPack: an integrated NMR approach to RNA structure determination. Methods 25:316–332
45. Kallansrud G, Ward B (1996) A comparison of measured and calculated single- and double-stranded oligodeoxynucleotide extinction coefficients. Anal Biochem 236:134–138
46. Stonehouse J, Clowes RT, Shaw GL et al (1995) Minimisation of sensitivity losses due to the use of gradient pulses in triple-resonance NMR of proteins. J Biomol NMR 5:226–232